Cavern and Tunnel Collapses due to Adverse Structural Geology

Colapsos en Túneles y Cavernas debido a Geología Estructural Adversa

Nick Barton
NB&A, Oslo. nickrbarton@hotmail.com

ABSTRACT: *Some remarkable cavern and tunnel failures are described in this keynote paper. As an independent consultant one occasionally has the privilege of observing some dramatic effects of adverse and usually completely unexpected structural geology, causing tunnel or cavern failures that can be dramatic. Very regrettably, the collapses are sometimes fatal for some unsuspecting tunnel or cavern workers. There is often an adverse design for the special circumstances. Failure is most frequent during construction, with only the temporary support to resist the unexpected challenges of adverse structural geology. In fact the three most serious cases shown have lattice girders or steel arches as one of the components of the temporary support. It is usually a surprise to read that this hardest of materials provides the softest of deformation resistance, because of the difficulty of making contact with the uneven and by now blasted rock surface, once the soil and saprolite has been passed in the early tens of meters of a typical tunnel. These partly free-standing girders or arches, and their footings, deform too much before fully resisting radial deformation, thereby potentially reducing the shear strength of the rock mass, which may not be bolted when there is deep weathering. Such measures (lattice girders and steel sets) should never be part of the Q-system, which is essentially for excavations in rock masses, even if of poor quality with clay and fault zones. A bolted, and intimately supporting, steel-and-fiber reinforced S(fr) arch is needed to reduce the risk of collapse. This can function well even when there is an excessively rough perimeter due to over-break.*

RESUMEN:

En esta charla especial se describen algunas colapsos notables de túneles y cavernas. Un consultor independiente de vez en cuando tiene el privilegio de observar algunos efectos extraordinarios resultantes de una geología estructural adversa y completamente inesperada, capaz de causar colapsos substanciales en túneles y cavernas. Muy lamentablemente esas colapsos son algunas veces fatales para algunos trabajadores no conscientes de la presencia del peligro. Hay con frecuencia un diseño adverso para una circunstancia especial. Los colapsos ocurren a menudo durante la construcción, cuando se emplea solamente un soporte temporal para resistir los retos inesperados de una geología estructural adversa. En realidad, los tres casos más serios presentados tienen vigas de celosía o arcos de acero como uno de los componentes del soporte temporal. Por lo general es una sorpresa saber que estos materiales tan duros proporcionan la peor resistencia a la deformación, por causa de la dificultad de tener contacto adecuado con la superficie irregular de la roca dejada por las voladuras y una vez se ha traspasado el suelo y el saprolito en las primeras decenas de metros en un túnel típico. Estas vigas de celosía o arcos y sus zapatas, actuando parcialmente libres, se deforman demasiado antes de que puedan resistir plenamenete la deformación radial, reduciendo así potencialmente la resistencia al cizallamiento del macizo rocoso, algunas veces no apto para el empleo de pernos cuando hay una alteración profunda. Tales complementos (vigas de celosía y arcos de acero) nunca debem ser parte del sistema Q, que debe ser esencialmente para excavaciones en macizos rocosos, aunque sean de mala calidad y con zonas de arcillas y de fallas. El uso de hormigón proyectado con pernos y reforzado con malla y fibra de acero S(fr) es necesario para reducir el riesgo de colapso. Esto tipo de suporte puede funcionar bien, incluso cuando hay una superficie muy rugosa por causa de exceso de excavación o de voladuras.

1. INTRODUCTION TO NATM

Because of the cost and time involved in construction, and the fact that double-shell NATM tunnels and caverns are used in prominent transport projects, such as motorways, metro-stations, and high-speed rail tunnels, they are the frequent subject of conference papers and tunnel magazine articles. The description 'double-shell' is used to imply that a final concrete lining will cover the temporary support phase of (typically) lattice girders, mesh-reinforced shotcrete, and rock bolts. There are variations of the latter involving fiber-reinforced shotcrete (generally a superior choice) and no rock bolts (an adverse choice, though if rock cover is absent, this is necessary unless self-drilling bolts are used.). Typical sequences of NATM are shown in Figure 1a and 1b, from the Austrian Society of Geomechanics NATM method statement of 2010.

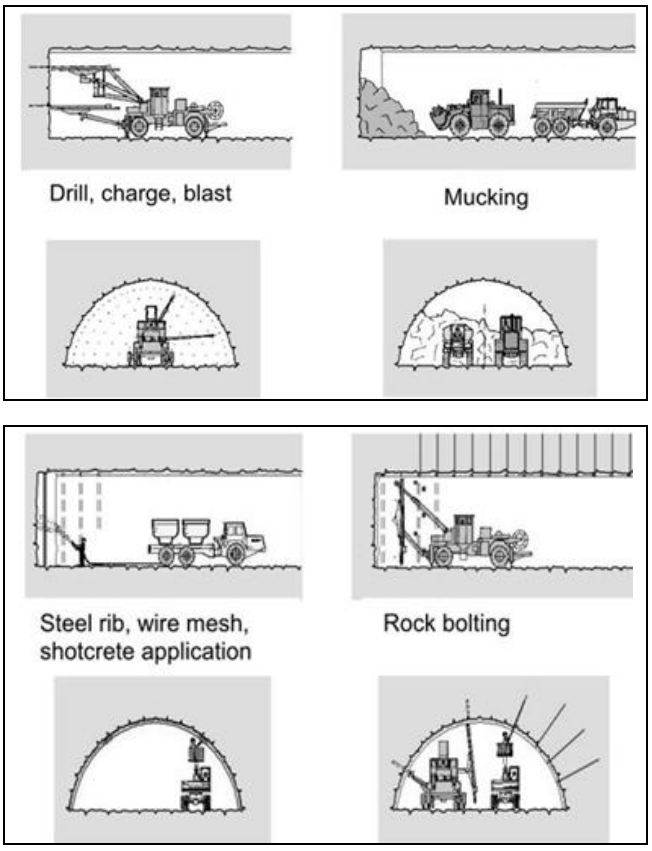

Figure 1a. Top-heading phase of NATM with 'steel rib, wire mesh, shotcrete application' and rock bolting. This is a critical phase if the choice of tunneling method is double-shell NATM. One should not delay with rock bolting. This is especially important when reaching jointed rock, when over-break makes lattice girders less reliable.

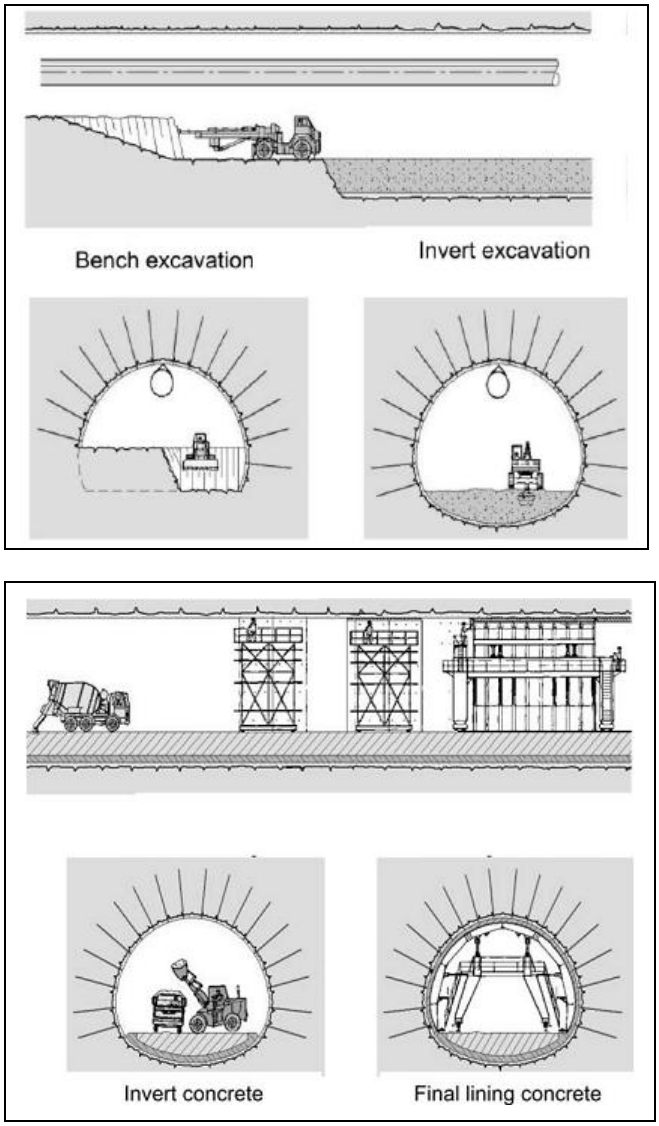

Figure 1b. Benching down, invert, and final concrete lining. This follows the fixing of a drainage fleece and membrane. A labour intensive method which is several times as costly as the more commonly used single-shell NMT. (NATM: The Austrian Practice of Conventional Tunnelling', ASG, 2010).

2. INTRODUCTION TO NMT

Observant readers will have noticed the 'more commonly used' reference to NMT in the above NATM figure caption. This is because single-shell B+S(fr) (permanent bolting and fibre-reinforced shotcrete) which is most frequently chosen with the help of the Q-system, is such a common method in hydropower tunnels, mine roadways, hydropower caverns, and countless road and rail tunnels in many countries. Of course the RMR rock mass description method of Bieniawski is also a source of support class selection for many single-shell

excavations. The fact that such single-shell tunnels are constructed so much faster and more cheaply means that they are less frequently to be found in the pages of tunneling journals. The designers and contractors have probably moved on to other projects. Note that the world record for a completed single-shell tunnel is presently 5.8 km in 54 weeks (104m/week single face mine access tunnel) with a peak of 150 m in one week. The tunnel section was 38m^2, in coal-measure rocks with some B+S.

3. CONTRASTING NATM/NMT OPERATIONS

A simple way to illustrate the differences between so-called 'conventional NATM tunnelling' and conventional NMT tunneling, is to use some illustrative photographs. We will see some shotcreting of lattice girders in a cavern, prior to the planned concrete lining phase: a double-shell project. As contrast we will see some single-shell B+S(fr) work in a large rail tunnel. This has been systematically pre-injected, thereby improving the effective quality of the shales, limestones and igneous dykes, and providing a dry tunnel, at much lower cost despite pre-injection, than if by NATM.

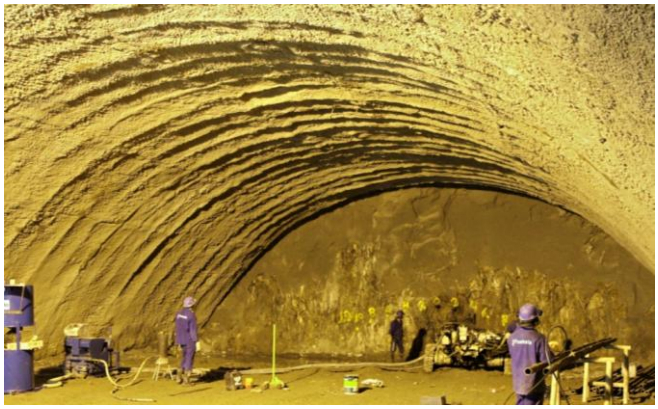

Figure 2. The temporary support phase of NATM, spraying in the lattice girders (unbolted due to low cover) and mesh.

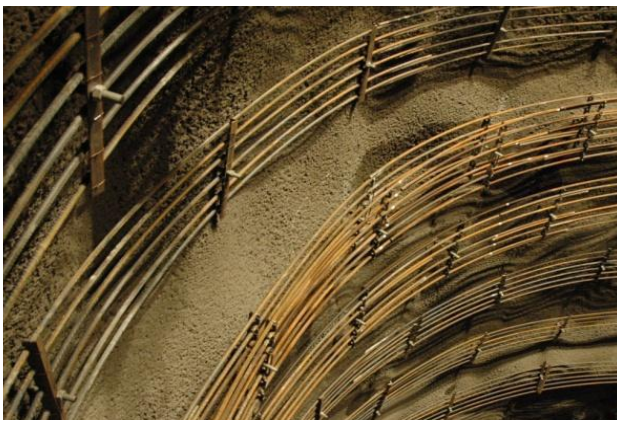

Figure 3. Top: a pre-injected high-speed rail tunnel, with the first layer of S(fr) and the permanent (5-way) corrosion protected bolting applied close to the face. Cautious 4m advance shown. Bottom: a road tunnel through a section of faulted rock. Note systematically bolted (16 mm bar) ribs, prior to spraying thick individual RRS (rib-reinforced shotcrete) arches. Figure 4 shows the important sequences involved.

In the case of the NMT tunnels illustrated, the initial support and reinforcement is finalized while progressing the tunnel. There is no unsafe, temporary support phase, waiting many months or even 1 or 2 years for a final (and finally safe) concrete lining, as in NATM. Risk is high in this phase.

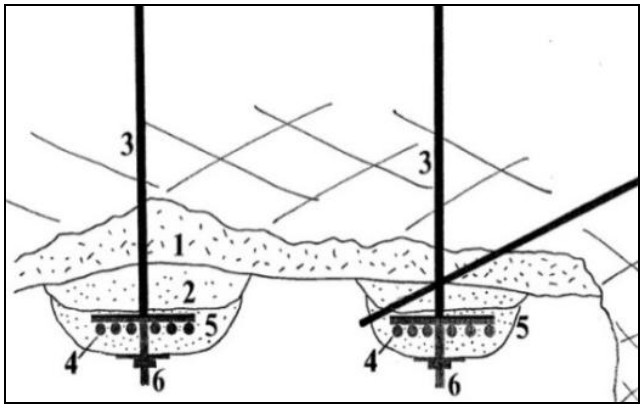

Figure 4. The principal of RRS. This is a much sounder scientific method than unbolted, deformable lattice girders.

In the Grimstad and Barton, 1993 and Barton and Grimstad, 1994 updates of tunnel and cavern support methods using the Q-system, we suggested the need to change S(mr) to S(fr). At this time, attention was drawn to the monitored results shown in Figure 5a. Ward et al. 1983 had monitored different tunnel support methods in an experimental tunnel in mudstones, at the Keilder project in NE England. The obvious advantages of immediately combining B+S (not even mesh- or fiber- reinforced shotcrete) were very clear reasons why steel sets (or lattice girders) had never/will never, be intended components of Q-based NMT support.

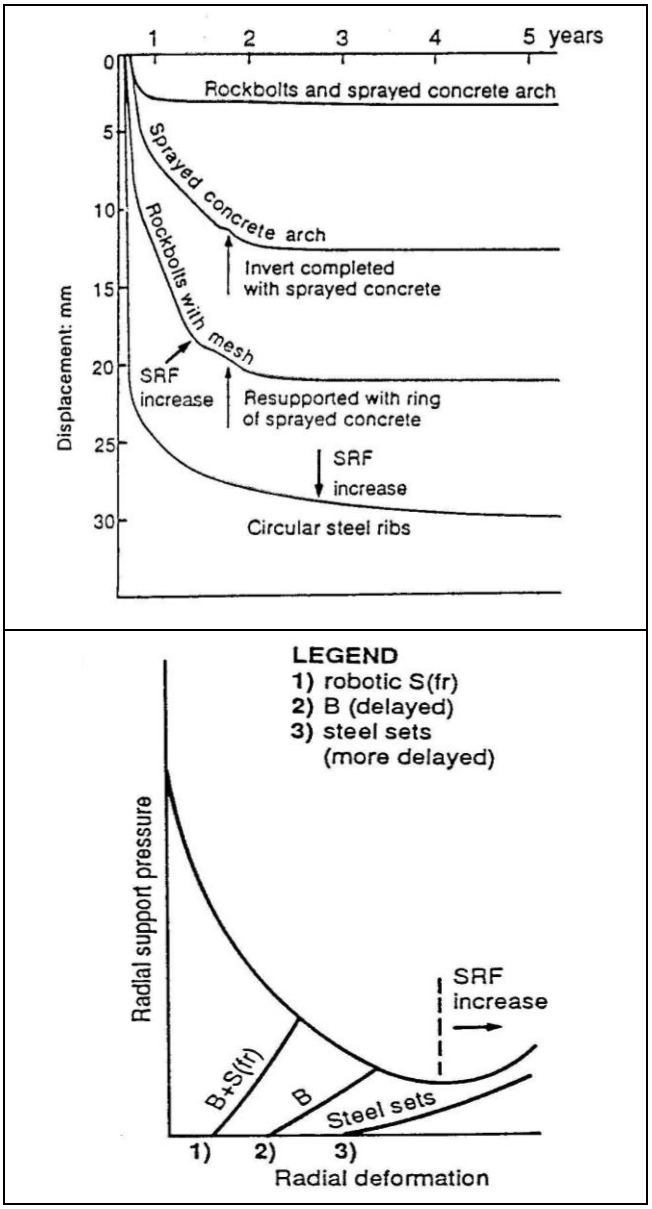

Figure 5. Avoidance of steel sets (or lattice girders) was and remains, an important advisory for NMT Q-system users.

4. COLLAPSE OF PINHEIROS CAVERN

Even the robust 25 x 25 x 32mm bars constituting the lattice girders shown in Figure 2, which were sprayed in with 40 to 50cm thick S(fr), proved insufficient to resist a completely unexpected and probable 15,000 tons load of rock and relic-jointed saprolite. This lay undetected above 35-40m length of the cavern arch. Six boreholes failed to detect it.

Figure 6. Collapse of the 20m span Pinheiros metro cavern while under construction in early 2007. The pre-grouting tubes in collapsed rock, and the folded lattice girders, were the result of a concealed 10-11m high ridge of better quality rock, which was missed by adjacent investigation boreholes.

The principle of the loading mechanism is illustrated in Figure 7b, but more geologic reality is shown if we borrow the classic drawings of Linton, 1955, who was describing the origin of 'tors' (towers of jointed granite) in SW England. His structural geological drawings are reproduced in Figure 8. In the case of the metro station cavern collapse, the second sketch (8b) applies: a concealed ridge of less weathered rock. Barton, 2009.

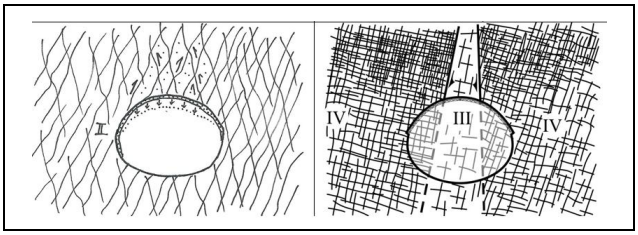

Figure 7. Sketches of potential 'wedge' loading on lattice girders. In the case of sufficiently low shear strength and low dilation the left-hand case could severely load the support. Resisting such a mechanism would require bolting and anchoring. In the case of the collapse illustrated in Figure 6 it was the loading from the ridge of (Bieniawski) class III rock, which was preserved as a 10 to 11m high ridge above the cavern centre-line. The potential for such a ridge is shown in Figure 8b, i.e. ridges that are still concealed by soil and sand.

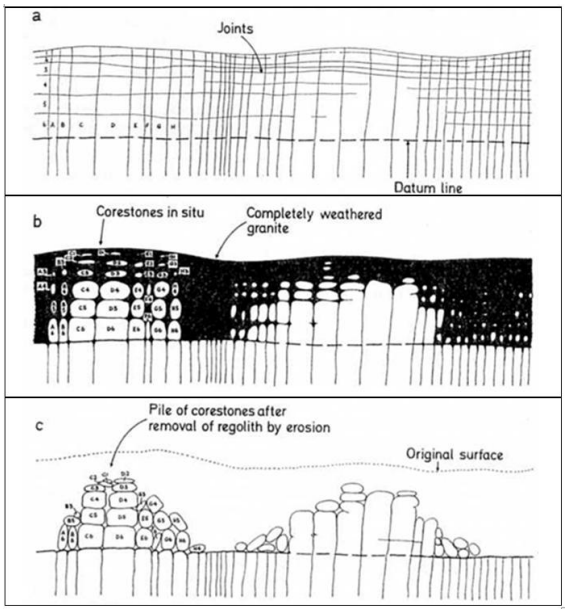

Figure 8. Linton, 1955 drawings showing the origin of 'tors'. In the case of the hidden ridge of rock that caused the São Paulo metro station cavern collapse, the second stage applies.

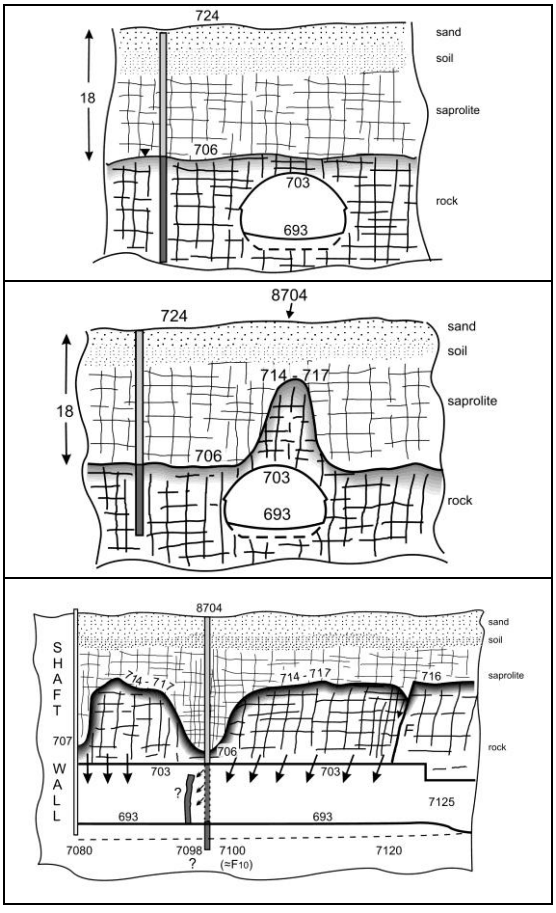

Figure 9. Top: the rock cover assumption based on five boreholes. Centre: the 'reality. Bottom: the reason that the borehole drilled on the cavern centre-line missed the ridge of rock. The ridge of rock fell 8 to 10m crushing the support.

Figure 10. The fateful central borehole (8704) also showing 18m of sand and clay cover, and only 3m of rock cover.

Figure 11. The tragic Pinheiros station cavern collapse, which took the lives of seven people who had been walking or driving along the suddenly collapsing Rua Capri (on right)

The above case from São Paulo was the result of a totally unknown and unexpected non-uniform loading. Triggering may have been due to local crushing of weathered rock beneath a limited

Figure 12. The curved appearance of the jointed ridge of rock, which was exposed after half a year of excavation. The sides could be penetrated 1 to 2 cm with gentle blows of a geological hammer. Friction was therefore low. This ridge was traceable for 25 to 35 m length, and had fallen 8 to10m to the cavern floor, above the crushed and folded support.

number of 'elefant footings'(in 'left' sidewall) and immediate release of huge unbalanced forces. This was possible due to the suspected shear of a major planar discontinuity at the far end of the ridge of rock (F: Figure 9c, and Fig. 15). Significantly, this was crossed by a flowing-at-the-time-of-failure storm drain. Joint water pressure and softening of clay-coatings during shearing, may have triggered the pending instability and sudden failure.

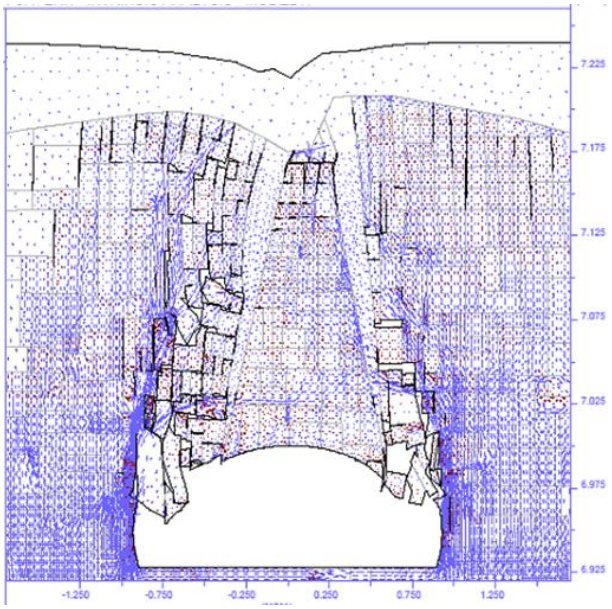

Figure 13. Intrinsic (unsupported) failure mechanism, based on the consistent geological logging of Class III in the centre of the cavern face, and class IV on either side. Dr. Stavros Bandis UDEC modeling, reproduced in Barton, 2009.

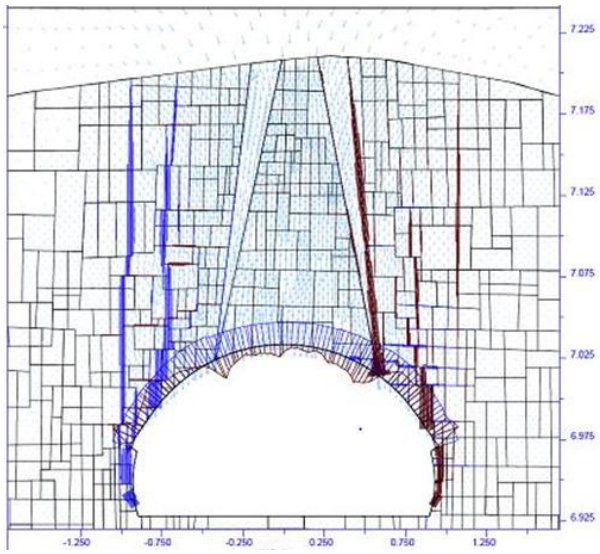

Figure 14. Overloaded plastic hinges from the N-M interaction diagram. Downwards shearing of the ridge-of-rock, with assumed low friction boundaries of increasing thickness in the weathered zone. Bandis UDEC model, in Barton, 2009.

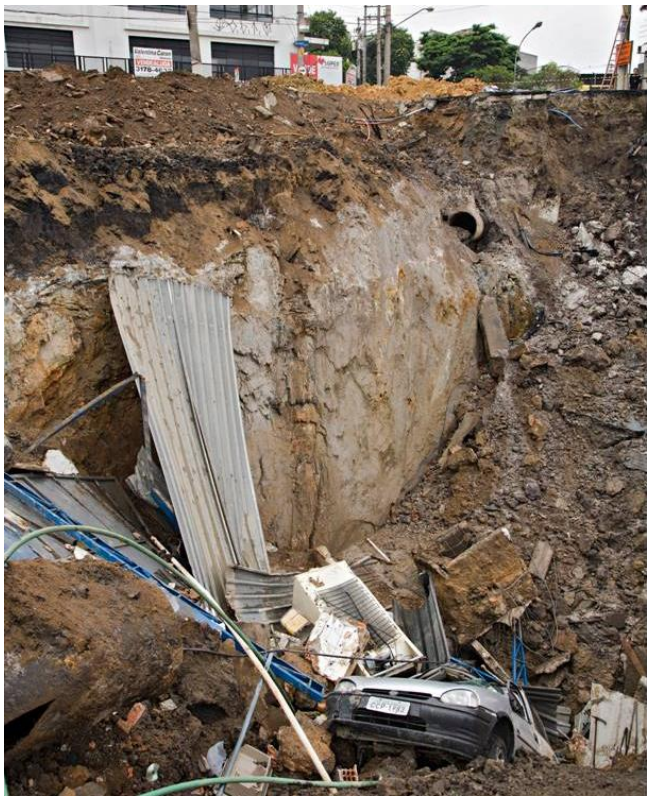

Figure 15. The storm drain cut by the sheared discontinuity (F) marking the end of the failed area, furthest from the station shaft construction seen in Figure 11.

5. AN OPTIMISTIC TEMPORARY NATM SUPPORT

The second major failure to be briefly presented occurred 'somewhere in South America', and involved the failure, first of 140 m of a three-lane 20 m span motorway tunnel in soil, saprolite, then anisotropic (phyllite) rock, followed some months later by the complete failure of 140 m of the parallel tube, which of course showed signs of shearing and over-loading with the loss of its neighbor.

An optimistic design with under-dimensioned lattice girders, and unreinforced shotcrete, though of specified minimum 30cm (and up to 60 cm) thickness, but no bolting even when in rock, indicated that the designer was expecting 'uniform conditions'. In fact axi-symmetric models, with no consideration of an initially sloping (lateral) hillside proved to be one of the key weaknesses.

Photographs of the collapse as seen in the portal area in Figure 16. Representation of the influence of adverse structural geology in UDEC and 3DEC, as performed by Dr. Stavros Bandis, are illustrated in the next series of figures.

Figure 16. Top: First the outer, right-hand, 20 m wide motorway tunnel failed, with failure progressing back-wards, towards the portal, as a result of an unexpected structural geological detail at approx. ch. 130 m, not seen beneath dense forest. Bottom: many months later, the over-strained parallel 20 m wide motorway tunnel also failed, making 280 m of tunnel lost in total. The contractor was compensated.

As may be suspected from Figure 16, the twin-tunnels started in soil, then saprolite. Here, lattice girders are an accepted method. However, when rock is reached, and blasting is needed, several potential problems for lattice girders arise. Firstly, there is likely to be over-break, and then any continued use of (unbolted) lattice-girders is faced with the challenge of contact with the rock, footing deformation, and potential 'point-load' deformations in the (nearly) shotcreted girders.

The loading is unlikely to be uniform anymore, and strongly anisotropic and inhomogeneous loads are likely. Remember: 'anisotropy is everywhere' in rock masses, due especially to joint stiffness inequality: $k_s << k_n$ often 1/50 to 1/100. Figure 17 is a view into the parallel top-heading, the one that failed many months later, due to anisotropic loads.

Figure 17. The top-heading of the parallel tube, which failed completely (140 m) many months later. Note the 'bulges' of the shotcreted lower side-drifts, seen in the numerical models illustrated in the following three figures.

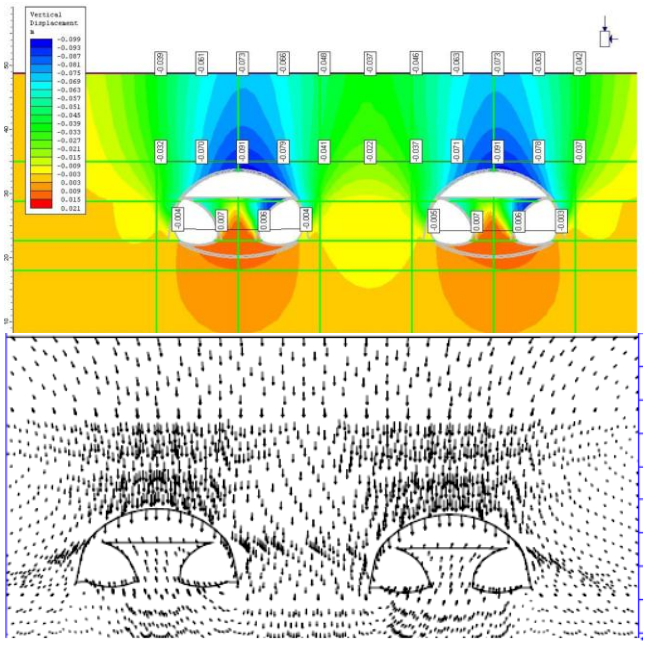

Figure 18. Optimistic (and lazy) isotropic continuum and axi-symmetric models, which ignored the effect of the adjacent sloping hillside, shown with different results, in Figure 19.

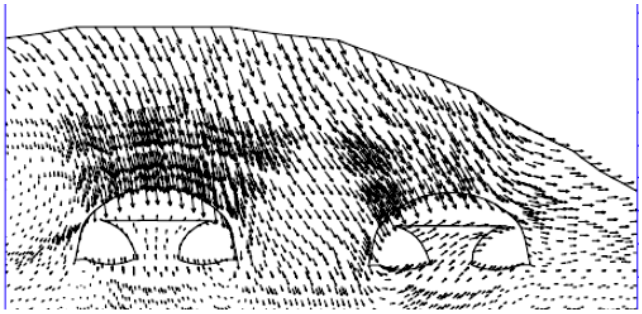

Figure 19. The two-dimensional 'reality', still with isotropic continuum behavior, suggests that more robust tunnel support should have been designed for the outer tunnel. When the actual anisotropic phyllite and weathered dike is also modeled: see its dramatic potential influence in Figure 20.

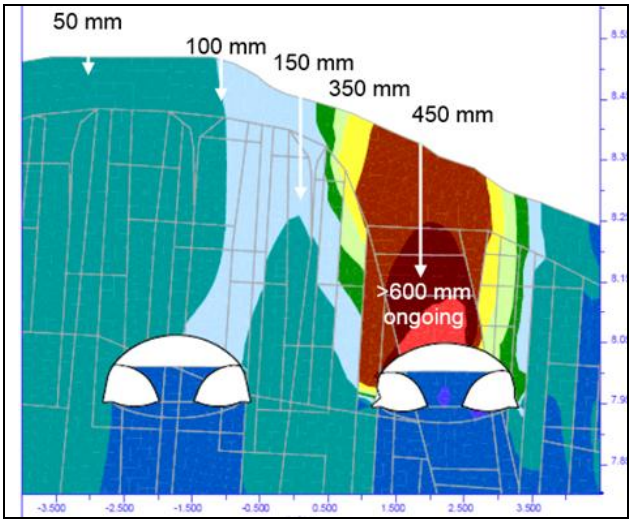

Figure 20. Some two-dimensional 'reality', with a UDEC model incorporating anisotropic behavior from sub-vertically jointed phyllite. The model also incorporates an important structural geological detail: a vertical, deeply-weathered dike Tunnel failure is on-going, due as usual, to multiple reasons, including inappropriate-design-in-the-circumstances. All the UDEC and 3DEC modelling (Figures 18b, 19, 20 and 23) was performed by my colleague Dr. Stavros Bandis.

Figure 21. The weak and anisotropic appearance (and behaviour) of phyllite, as seen in the neighbourhood of this tunnel.

When 140 m of the first tunnel collapsed, it was triggered some 130 m into the tunnel by the anisotropic state of the rock mass, and by an inappropriate 'uniform-load' assumption. There were no rock bolts, as in single-shell Q-system based B + S(fr), so uneven loading, which had to be assumed, had every possibility of over-coming the 'soil and saprolite' lattice girder design. Presumably there were inherent weaknesses, as the whole 140 m of the tunnel collapsed, fortunately when all workers were out of the tunnel. Figure 22 shows some details at the surface, after the second tube failed.

Figure 22. A deep tension crack and rotation of the road surface, trees and pole, after the second tube had collapsed.

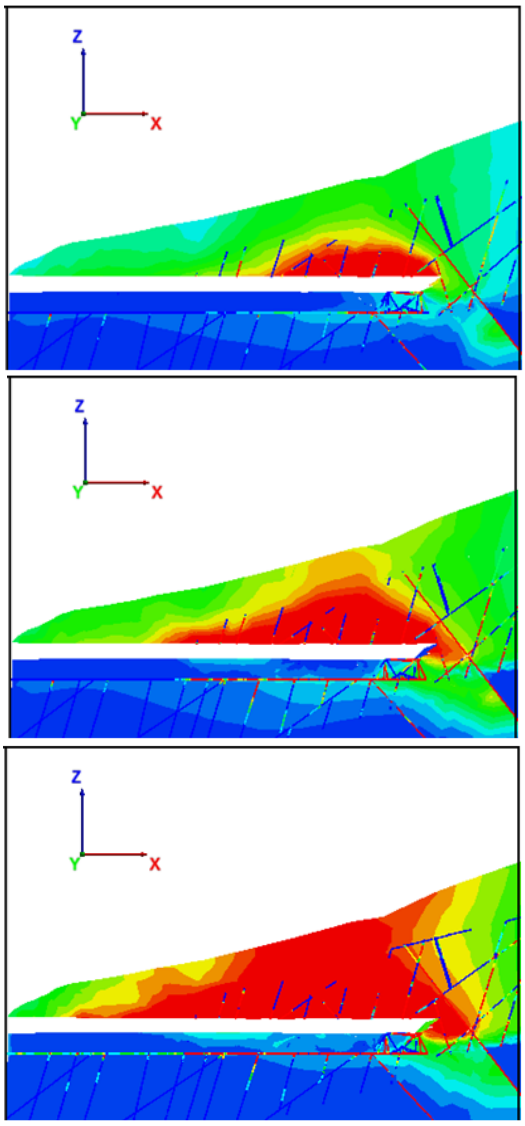

Figure 23. Retrogressive collapse of the outer first tunnel, as modeled in an anisotropic 3DEC. The second tube may have suffered a similar 'regression', triggered parallel to the weak dike that is believed to have initiated collapse of tunnel #1.

6. STEEL SETS FAIL AT A FAULT ZONE

A third major collapse, regrettably taking the lives of a group of cavern workers, is shown in the following figures. Being part of a major hydroelectric project, the cavern where the sudden collapse occurred was a not yet completed D/S surge chamber, which would eventually have been 60 m in height. It was one of three major excavations, as shown in Figure 24. At the time of failure it had a sloping invert and had reached a height of ≈ 30 m.

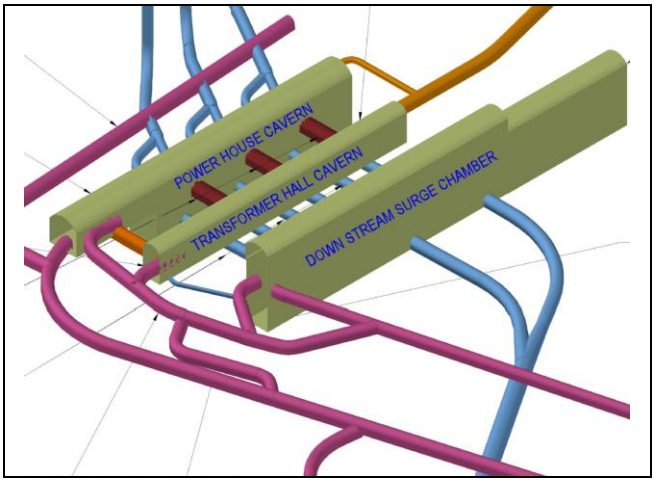

Figure 24. A hydroelectric project 'somewhere in Asia', suffered a major initial collapse, followed by successive falls from the fault-affected void above the arch.

Figure 25. The initial sudden collapse of approximately 35,000 m^3 regrettably buried a group of cavern workers.

Figure 26 shows the effect of attempting to remove some 15,000 m^3 in order to try to recover the bodies of the six victims. The extent of the destruction of the steel-sets in the arch was thereby revealed. There was subsequently a major additional collapse, and raveling continued intermittently, resulting in the 're-filled-with-new-debris' appearance shown in Figure 27.

Figure 26. The attempt to remove some 15,000 m^3 of the fallen rock, revealed the destruction of the 'heavy' steel sets in the arch, which are seen from some 30 to 40 m distance. There is a faulted zone in the left-side of the arch.

Figure 27. Further major falls contributed even more to the collapsed material, which was believed to be as much as 70,000 m^3. There may now be a cavity with approximate dimensions L x H x W of (50-60) m x (40-50) m x (30-35) m. Special measures were proposed for its stabilization, so that the fallen rock can finally be removed, and the project completed. A long delay must obviously be expected.

When evaluating the reasons for the huge collapse, it appears that the unchanged arch support when encountering a faulted zone in the arch, may be the reason for the sudden and then progressive collapse. Tangential stress could not be sustained.

At the Mingtan pumped storage project in Taiwan, the known presence of some thirteen clay-bearing 'bedding-plane-faults, dipping at 30° and

striking perpendicular to the machine-hall axis, resulted in a major 'clay-replacement-with-concrete' project, set in motion by Taiwan consultant Sinotech. (Hoek, 1991). The thickest clay layers between the faulted beds of sandstone were some 2 m thick. This ensured a cavern 'rock-and-concrete' arch of many meters thickness, capable of generating and sustaining elevated tangential stress. In the walls, down-wards and back-wards inclined anchoring and bolting was advised and used, to ensure sufficient shear strength in the faulted (but un-concreted) walls. (Barton, 1994).

7. LIMITATIONS OF LATTICE GIRDERS

The use of lattice girders or steel sets is widespread in countries with many shallow tunnels in soil and saprolite, where loading is probably more easily estimated, and where excavation is gradual. For instance it is often set-by-set (girder-by-girder), with the latter placed at for instance 0.8 m c/c, and sprayed in with plain shotcrete, or S(fr), or the less quality-controllable S(mr).

If over-break is limited, good quality work can be performed. In one project where the writer was giving late advice, there was a big store of empty oil drums outside the portal. Their use? To fill the several meters of over-break, and 'make contact' between the rock and the steel sets and wood.

Figure 28. At one end of the deformable temporary support spectrum, and clearly a dangerous extreme, is the use of empty but closed oil drums, designed 'to fill' the several meters of over-break, and therefore placed above the steel-sets-and- wooden-planking. This is the most optimistic and dangerous tunneling practice yet seen. Figure 29 is the view from inside the tunnel. Optimism in the strength of wood?

Figure 29. The 'support' of optimists: oil drums and wood.

When the soil and saprolite sections of a tunnel have been passed, using lattice girders and shotcrete, and some form of top-heading-and-side-drift format, further tunnel advance may involve penetrating a very non-uniform-loading region of differentially weathered rock, with sudden weathered clay-, silt- or sand-bearing discontinuities.

It is in such transition zones that every effort should be made to pre-grout ahead of the tunnel face. The use of single-shell NMT, i.e. Q-value based B+ S(fr) + RRS (?) can then be commenced, speeding progress, reducing cost and specifically: reducing risk. To continue to rely on lattice girders and shotcrete, without rock bolts, is inviting the possibility/probability of non-uniform loading, and local failure, as in Figures 16 through 23.

Imagine for a moment the consequences of intersecting a dipping, continuous, and low-strength major discontinuity, such as illustrated in the granite quarry in Figure 30. 'Point-loading' of several lattice girders could easily exceed their strength. Bolting (and even anchoring) might be essential.

Figure 30. Note the scale of the geologists and the joints.

Figure 31. Unusual continuity of two major joint sets which could be intersected soon after passing over-lying saprolite. The likely depth of over-break, now due to drill-and-blast, should cause lattice girders to be replaced by B + S(fr), if worker safety, tunnel stability and cost remain as issues.

It is necessary to stop using (deformable) lattice girders when passing into jointed rock. Q-value based single-shell B + S(fr) (i.e. NMT) would be the appropriate, cheaper and safer method, because with the onset of drill-and-blast, there will be the possibility of deep over-break. It is this that specifically compromises the continued use of steel sets or lattice girders: good contact with the rock becomes difficult, and anyway the steel and the footings deform, inviting loss of rock mass strength. We need to worry about loss of strength in rock mechanics: perhaps also in soil mechanics.

Figure 32. A 'typically jointed' crystalline hard rock, in this case granite, often has three or more (locally-occurring) joint sets. It is found that when the Q-system's Jn/Jr ratio is ≥ 6, over-break is inevitable. Figure 33 shows an explanation.

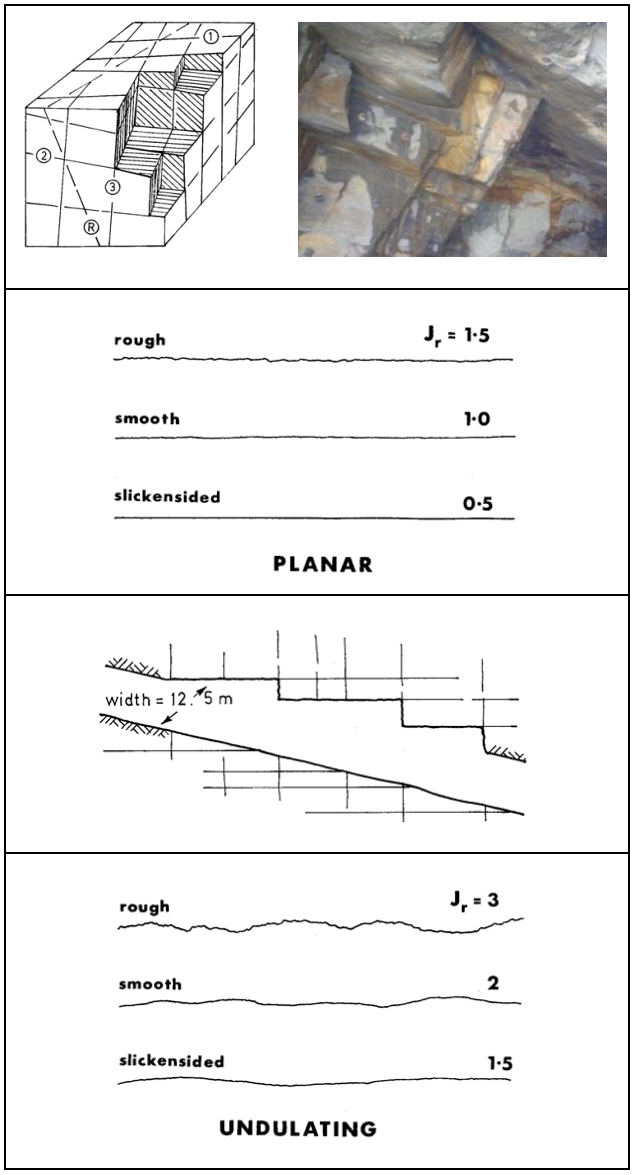

Figure 33. The over-break criterion of Jn/Jr ≥ 6 (Barton, 2007). This is now actively used by contractors in claims. For instance: 6/0.5, 9/1, 9/1.5, 12/2, 12/1.5 for two sets plus random, three sets, and three sets plus random: each cause over-break. On the other hand 12/3 and even 15/3 prevent it, due to the stabilizing effect of dilation when joints are rough.

8. OVER-STRESSED / OVER-STRAINED

Having concentrated so far on insufficient shear strength, insufficient designed support, and gravity-assisted (massive) failures, each at moderate stress levels, it is appropriate to end this paper with some examples of failures caused by high-stress. Since *we always need to compare stress with strength*, and are part of a 'soft rock' symposium in Cartagena, Colombia, the 'high-stress'

could be as low as 1 MPa, (or as high as 100 MPa if hard rock). We will see real and modelled failure of chalk marl and volcanic tuffs, where uniaxial strengths are in the range of approximately 3 to 9 MPa, and tensile strengths << 1MPa. A 'stress-induced' (or initially strain-induced) failure from the earliest TBM Beamont Tunnel of 1880, adjacent to the UK-France Channel tunnel will be shown. We will also see failures in the large spans of some underground churches, in the Cappadocia tuffs of Turkey, with similarly low UCS and tensile strengths.

Due to recent ultra-simple discoveries by Dr. Baotang Shen (CSIRO, Australia), we need to also address the (extensional) strain caused by the 'high stress'. Poisson's ratio and the tensile strength may play an important role due to a *critical tensile strain* that can cause tensile failure in intact rock, even when all boundary stresses are compressive.

Dr. Shen has found that the commonly occurring ratio of σ_θ/UCS ≥ 0.4 marking the onset of fracturing around underground openings in brittle rock, has an alternative explanation. (σ_θ/UCS is the ratio of the maximum elastic-isotropic tangential stress and the uniaxial compressive strength).

Table 1. The extensional strain logic of Dr. Shen.

$\varepsilon_3 = [\ \sigma_3 - \nu(\sigma_1 + \sigma_2)\ ] / E$ (3D stress/strain)	$\varepsilon_3 = [\ \sigma_3 - \nu.\sigma_1\ ] /E$ (2D stress/strain)

When $\nu(\sigma_1 + \sigma_2) > \sigma_3$, (negative) extensional strain ($-\varepsilon_3$) will occur.	When $\nu.\sigma_1 > \sigma_3$ (negative) extensional strain ($-\varepsilon_3$) will occur. If (-) $\varepsilon_3 >$ - ε_c (critical) = tensile failure. $-\varepsilon_{crit} = \sigma_t/E$

At tunnel wall, $\sigma_3 = 0$, and $\sigma_1 = \sigma_{max.\ tang.\ stress}$
Therefore (-) $\sigma_t/E = \varepsilon c = (-)\ (\nu.\ \sigma_{tang.\ critical})\ /E$

(Next: eliminate the common Young's modulus **E**)

$\sigma_{tang.\ critical} = \sigma_t / \nu \approx$	$\frac{UCS}{10\nu} = \frac{UCS}{10 \times 0.25} = 0.4 \times UCS$

Note: Due to typical ratios of σ_c/σ_t (or UCS/σ_t) ≈ 10, and typical values of Poisson's ratio ≈ 0.25, the commonly occurring onset of extensional failure (and acoustic emission in a laboratory triaxial test) is when reaching an axial (i.e. 'tangential') stress ≈ 0.4 x UCS. Both in a triaxial test and around a circular tunnel, the initial extensional strain-induced tensile fracturing will tend to coalesce and propagate in unstable shearing. See FRACOD models which follow later.

So σ_θ/UCS ≥ 0.4 marking the onset of 'stress-slabbing' can be explained by $\sigma_t/\nu \approx 0.4$ following Table 1 extensional strain logic (see Shen and Barton, 2016 in press). A previously assumed scale-effect on UCS (≈ x 0.4) is not required, though no doubt is still occurring. Figure 34 shows the data.

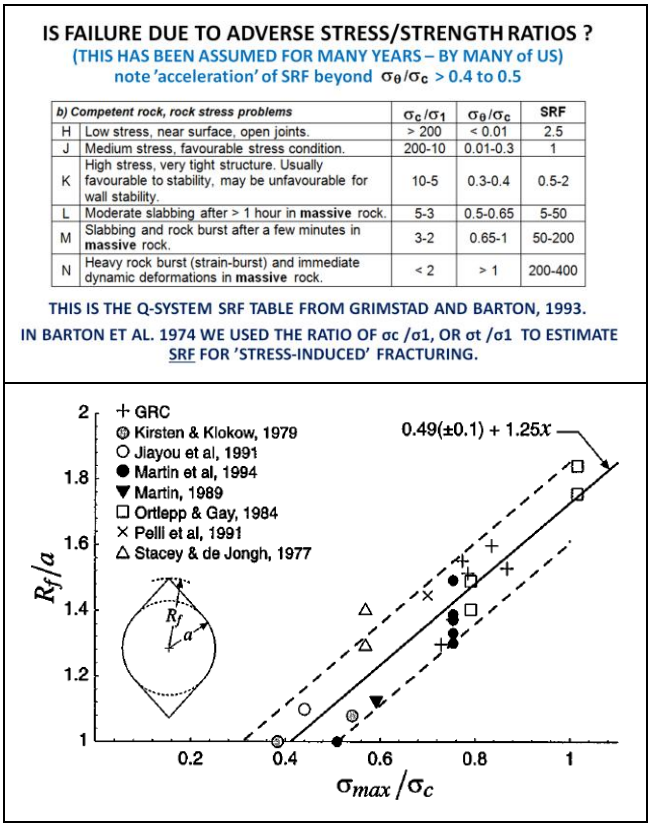

Figure 34. Top: The 'accelerating' value of SRF when the ratio σ_θ/UCS ≥ 0.4, from the Grimstad and Barton, 1993 analysis of deep (600 to 1,400 m) road tunnels in Norway. Bottom: an independently derived assembly of mining and nuclear waste URL research cases, from Martin et al.1999.

9. SOFT ROCK BEHAVIOUR, MODELING

This paper will be concluded with some soft rock behaviour / soft rock simulation / soft rock modeling, to demonstrate the effect of over-stressing and/or over-straining rock that, although soft, is still brittle enough to sustain jointing or fracturing. A nice starting point is the UK-France Channel Tunnel chalk-marl. This was originally assumed to be free of jointing as UCS was only 4 to 9 MPa. The reality, as demonstrated with a difficult leaking and over-breaking early weathered section under the sea (ch. 20-24 km), had locally well jointed conditions, and remarkably planar joints. The following was typical: RQD/Jn x Jr/Ja x Jw/SRF =

100/9 x 1/1x1/1 = 11. (Barton and Warren, 1996). In leaking weathered sections Ja was 2 and Jw was 0.66, which caused troublesome over-break, due especially to Jn/Jr > 6, adverse Ja and pressurized seawater. The over-break was very adverse for the unbolted (wedge-lock) PC segments used on the English side of this major triple-TBM project. The dripping seawater also created problems for the electronics and electrical systems on the TBM.

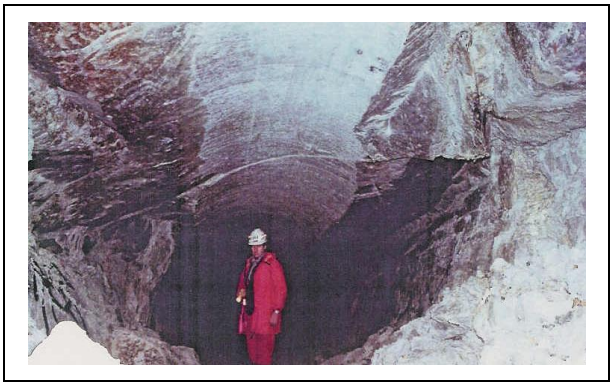

Figure 35. The earliest TBM driven tunnel, the Beaumont Tunnel from 1880, next to the UK-France Channel Tunnel. The chalk-marl has a UCS from 4 to 9 MPa. The tunnel depth changed from 50 m to 120 m, when passing below the 70 m high chalk cliffs. Note the bedding plane in the arch.

In the immediate neighbourhood of the Channel Tunnel tunnels, is the 1880 Beaumont 'pilot' tunnel (which stopped under the shore line). Here the rock was mostly more massive, and mainly affected by bedding planes. The stress/strain induced failure of this tunnel, where it passed from 50 m cover to 120 m due to passing under a 70 m high chalk cliff, is illustrated in Figure 35.

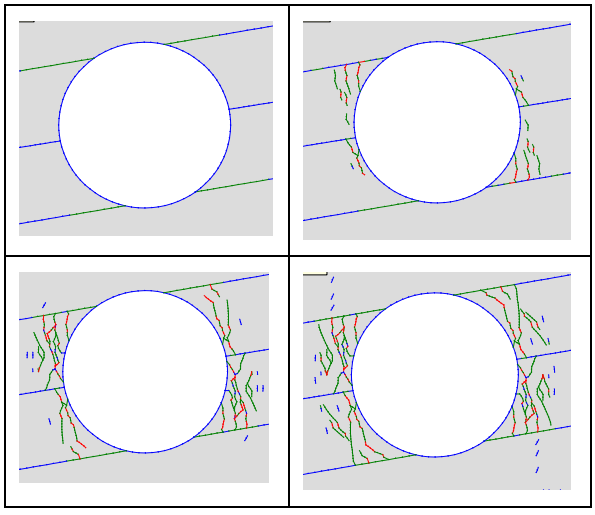

Figure 36. FRACOD model: chalk-marl with σ_h/σ_v = 0.33. The fracturing was the result of the 50 m increment of depth.

An important method for numerically modeling such stress/strain events is the BEM fracture mechanics code developed by Dr. Baotang Shen. The capabilities of this versatile code were recently described in the slim text book by Shen et al. 2013. Dr. Shen kindly produced the models shown in Figures 36 and 37, convincingly demonstrating that the horizontal stress must have been low in order to explain the mode of fracturing shown in Figure 35. There was high vertical $\sigma_{max.\ tang.\ stress}$.

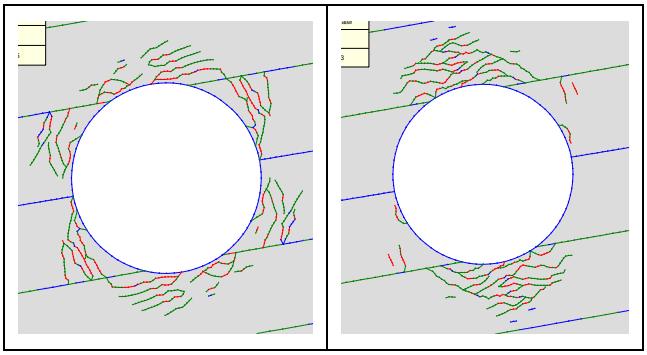

Figure 37. FRACOD models of chalk-marl, when assuming σ_h/σ_v = 1.0 (left) and 2.0 (right). These models clearly do not match the behavior seen in Figure 35, but otherwise perfectly demonstrate the importance of k_0 when modeling. (Note: red represents tensile cracking, and green represents shear).

There is a degree of 'log-spiral' shear failure (green) development in the FRACOD models, but this is partly 'frustrated' by the (assumed) presence of low-strength bedding planes, one of which is seen in the arch of the 2.2 m diameter tunnel, in Figure 35. The input data for these models were based on limited information, which required some estimation by the writer and by Dr. Shen. Principal properties assumed were as follows:

Table 2. Property for FRACOD	Value assumed
Young's modulus E	0.6 GPa
Poisson's ratio ν	0.25
Density d	2000 kg/m^3
UCS	6 MPa
Internal friction angle ϕ	30°
Cohesion c	1.73 MPa
Tensile strength σ_t	0.173 MPa
Fracture toughness K_{IC}	0.1 MPa m$^{1/2}$
Fracture toughness K_{IIC}	0.2 MPa m$^{1/2}$
Depth of cover	120 m
Vertical stress σ_v	2.4 MPa
$\sigma_H/\sigma_v = k_0$	0.33, 1.0, 2.0
Bedding plane dip, spacing	10°, 1 m
Bedding plane c and φ	0.0 MPa, and 20°

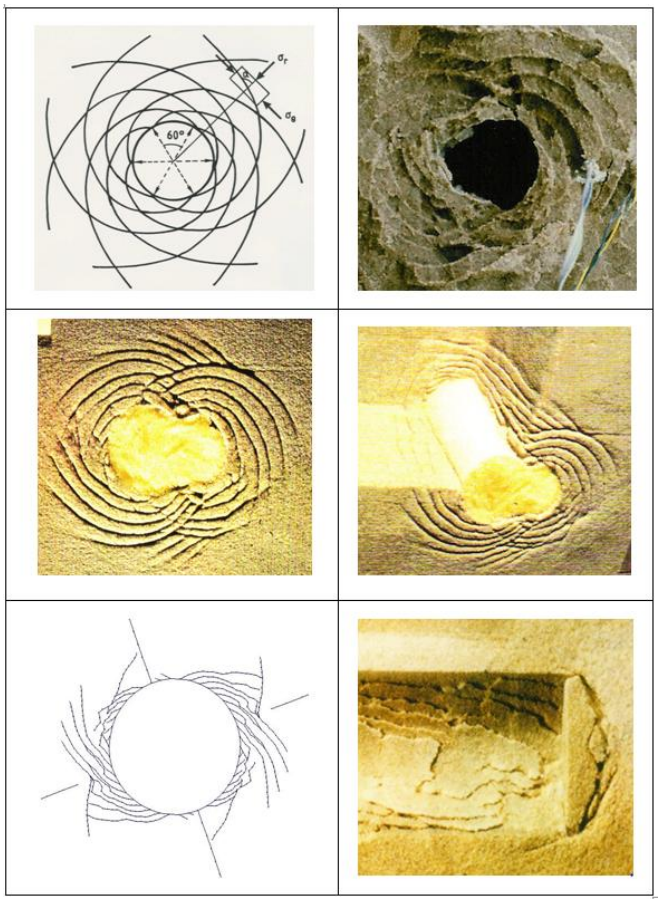

Figure 38. Panel 1: the log-spiral shear failure surfaces described by Bray, 1967. Panels 2, 3, 4, and 6: physical models of deep over-stressed boreholes (or model tunnels) showing in every case the propagation of failure in the form of log-spiral (shearing) surfaces, shown in cross-section, 3D cut-away, and longitudinal section. (These tangential shear deformations would be perceived as 'radial squeezing' from inside the model excavations. In reality they are not).

Severe over-loading of a weak rock, as illustrated in the physical models of Figure 38, will tend to result in the observation of 'squeezing'. The weak material may behave in a brittle manner, while undergoing extensive fracturing, equivalent to the higher-stress area of Figure 34. From 'inside the tunnel or borehole', large radial deformations and heavily loaded support (or the need for high mud pressure) is experienced.

Since the rock cannot generally be seen (it would fail without the heavy support or mud pressure), one may suggest that the 'squeezing' is often a manifestation of shear failures in the form of log-spiral surfaces of shear, as predicted by Bray, 1967. Log-spiral shearing was consistently experienced in the joint oil industry borehole (or model tunnel) physical modeling project, which we performed at NGI in the late 1980's. (See Addis et al., 1990). The writer was project manager, but the work was principally carried out by Addis and by my frequent co-author colleague Prof. Bandis from Univ. of Thessaloniki.

In every case the model boreholes/tunnels were drilled into polyaxially loaded cubes of uniformly cemented sand, with UCS = 0.5 MPa with $\sigma_1 > \sigma_2 > \sigma_3$ up to several times higher than the UCS. It was possible to drill inclined holes, non-parallel with the principal stresses, through steel flat-jacks.

(Panel 5 in Figure 38 is a FRACOD model of a 2 km deep (Trans-Andean) TBM tunnel in brittle rock shown, with two intersecting joints, and classic propagation of deformation/failure by log-spiral shear fractures. (Also Dr. Shen modeling),

10. THE SOFT TUFFS OF CAPPADOCIA

By good fortune, since just before attending a soft-rocks symposium, the writer very recently visited the incomparable region of Cappadocia in central Turkey, where Eurock 2016 was held. Figures 39, 40, 41, 42, 43, 44 and 45 give some very relevant images of the widespread practice of constructing tunnels, churches and even underground labyrinth-cities, for the mid-first millennium protection of tens of thousands of Christians. We were shown examples of stress/strain induced failures of large openings, by our knowledgeable Turkish guides Dr. ResatUlusay and Dr. Ömer Aydan, who kindly provided numerous technical articles describing their own and other's field and laboratory studies of the soft (UCS = 3 to 9 MPa) tuffs.

Figure 39. The ideal material for underground living.

Figure 40. Apparent extension failure parallel to σ_1. This 'cliff-face' failure mode is the cause of many openings being exposed. The small recesses are later additions, for pigeons.

Figure 41. Near-symmetric fracturing into the arch of a rectangular opening, seen in centre. Note extensive failures of the cliff face.

Figure 42. Far right: another rectangular opening, wide enough to eventually cause fracturing in the arch.

Figure 43. A large opening for a church, now exposed by (extension-strain) cliff failures. See detail of fracturing in the arch in the next photograph.

Figure 44. In view of the weakness of the rock, and the possibility of $k_0 > 1$ (i.e. acting along the cliff, especially in the arch), this fracture might have propagated in shear.

Figure 45. A rectangular opening with extension fractures.

Dr. Shen kindly modeled the 'test cases' shown in Figures 46 and 47, using properties largely suggested in the paper by Kasmer et al., 2013. In the case of the two fracture toughness values listed in Table 3, these were estimated, as in the earlier Beaumont Tunnel circular model that he kindly studied, in a similar 'quick response' mode.

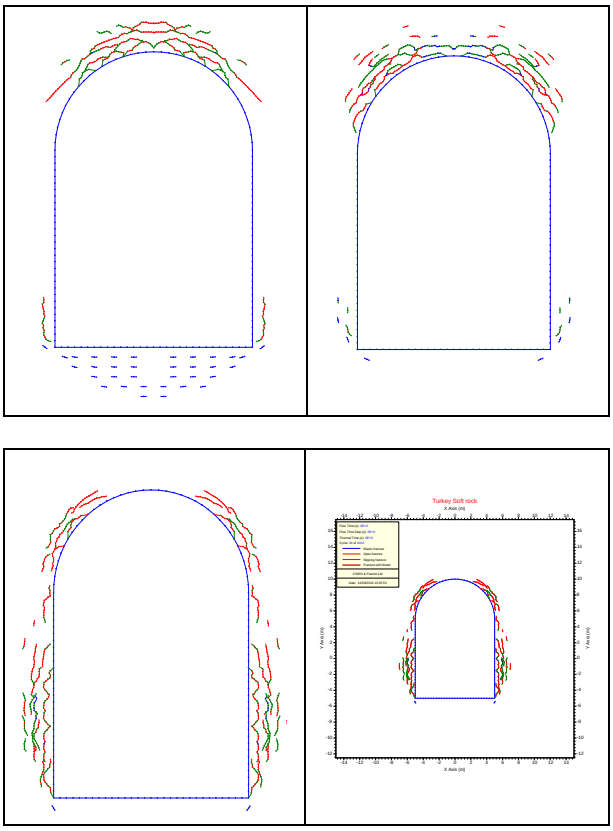

Figure 46. FRACOD models of ultra-shallow arched excavations in tuff (similar to Figures 43 & 44) with dimensions 10x15 m, and three stress ratios $k_0 = \sigma_h/\sigma_v =$ 2.0, 1.0 and 0.5.

Table 3. Input data assumptions for the Cappadocia tuffs.

Property	Value
Young's modulus E	0.6 GPa
Poisson's ratio ν	0.29
Density d	1290 kg/m^3
UCS	0.93 MPa
Internal friction angle ϕ	16.6°
Cohesion c	0.37 MPa
Tensile strength σ_t	0.04 MPa
Fracture toughness K_{IC}	0.05 MPa m$^{1/2}$
Fracture toughness K_{IIC}	0.1 MPa m$^{1/2}$
Depth of cover (from cave centre)	20 m
Vertical stress σ_v (at cave center horizon)	0.26 MPa (varied with depth, due to gravity)
Stress ratio σ_H/σ_v	2.0, 1.0, 0.5

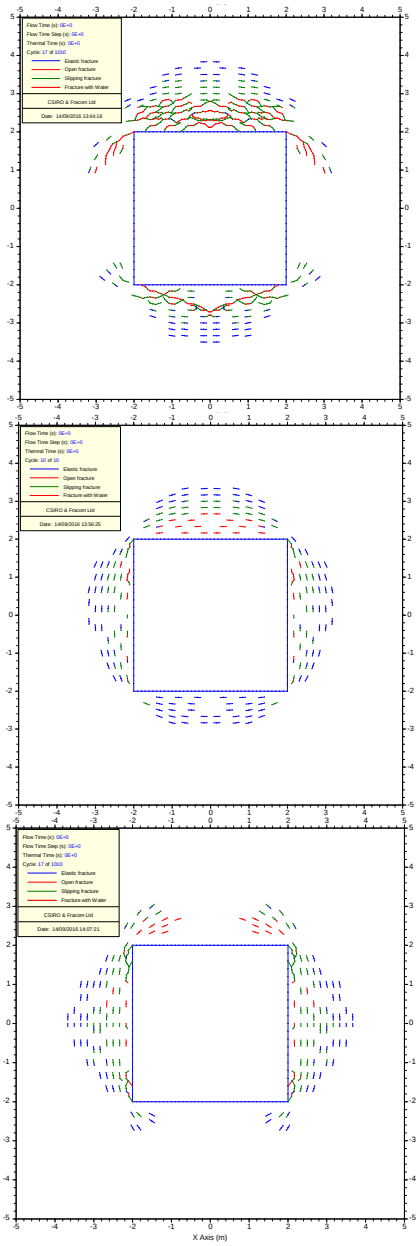

Figure 47. FRACOD models of shallow, square excavations (similar in principal to Figure 45) with dimensions 4x4m, and the three stress ratios $k_0 = \sigma_h/\sigma_v =$ 2.0, 1.0 and 0.5.

It is of interest to note that principal authors of technical articles concerning the Cappadocia tuffs are careful to point out the adverse effects of temperature cycles (an extreme shade-temperature range of approximately -20° to + 40° on properties such as UCS. They also point out the adverse effect of wetting and drying cycles. Careful study of the fracture 'colours' in Figures 46 and 47 reveal that the pervasive blue colour and distinctly short features are termed 'elastic fractures'. (Red = open in tension, green = shear). They would presumably, if reflecting reality, also 'assist' gradual degradation.

11. DISCUSSION AND CONCLUSIONS

This paper has addressed the possible reasons for some dramatic collapses of tunnels and caverns. Broadly speaking one could cite five technical reasons for the collapses, and the following could apply to collapses at many lesser scales, which 'fortunately' are more common than the dramatic cases illustrated here. The reasons for most tunnel and cavern collapses are attributable to excesses (too much or too little) *stress*, *strain*, *structure*, *strength* and *support*. The five 'S's'. Immediately one lists structure, the resulting anisotropic behavior becomes important. Even a single rock joint may impart a local anisotropy of stiffness (k_n/k_s) of something in the range of 10/1 up to 100/1 due to these very different normal displacement and shear displacement modes. Concerning stress, the previously assumed reasons for the importance of the ratio of maximum tangential stress compared to the uniaxial strength of the rock, has taken on new meaning, following the 'simple' finding by Dr. Baotang Shen, which is described stage-by-stage in Table 1.

The onset of fracturing is caused by extensional strain when reaching a tangential stress level given by (approx.) 0.4 x UCS, but actually caused by reaching the tangential stress level given by the alternative ratio σ_t/ν. For a very strong rock with UCS = 200 MPa, and an assumed σ_t of 20 MPa, a commonly occurring Poisson's ratio of 0.25 would suggest the onset of (extensional) fracturing when the isotropic-elastically assumed maximum tangential stress reached 80 MPa. At much higher (i.e. deeper tunnel) levels, propagation would be dominated by unstable and perhaps rock-bursting propagation in shear, higher up the 'diagonal' (Fig. 34).

For a medium strength 100 MPa rock, 40 MPa might apply, and for a weak 10 MPa rock, 4 MPa might apply, as the critical tangential stress for causing extensional fracturing. For the even weaker chalk-marl at the Beaumont tunnel (Figure 35) with UCS ≈ 5 MPa, we apparently need about 2 MPa to start the extensional fracturing. This is easily reached by the increment from the initial 50 m depth (no fracturing) to 120m depth, when the tunnel curves beneath the 70 m high cliffs close to the Channel Tunnel. In the case of the sometimes even weaker tuffs of Cappadocia: let us assume UCS ≈ 2.5 MPa, the σ_t/ν argument suggests that the 1 MPa tangential stress generated by 50 m high cliffs (with saturated rock density ≈ 2) is sufficient to generate extension fractures. If strength was reduced by 50% due to periodic saturation, 25 m high cliffs, as seen in most of the Cappadocia Figures 40, 41, 42 would be sufficient for failure to initiate. Of course the details of fracturing: the 'tentative' and highly discontinuous elastic fractures (blue), the tensile (red) and the shear (green) can be estimated by performing FRACOD models.

Progressing from 'intact' rock to the more commonly problematic rock masses, *the stress*, *strain* and *structure* are necessarily re-focused on the *strength* of the rock mass. Here we have to suggest a break with convention, because the different components of strength: the adversely oriented joint sets, some intact rock bridges, and perhaps some clay-filled discontinuities at less adverse angles, will each be mobilized at different levels of shear strain or shear displacement.

We cannot then add linear or non-linear variations of 'c' and σ_n tan'φ'. The reality is a cascade of shear resistence: intact bridges fail at smallest strain, the resulting new fractures (with high JRC, JCS = UCS and $\varphi_r = \varphi_b$ unweathered) shear next, followed by the 'capable' (adversely oriented) joint sets with their lower JRC, JCS and φ_r, followed by the peak (or residual) strength of clay-filled features at larger displacement (approximated by frictional strength $\tan^{-1}$(Jr/Ja).

Figure 48. Why did this largest of open-pit failures not take any lives and occur in two major events? Because it could be monitored: it failed progressively. (Not 'c' + σ_n tan'φ'). Many slope failures show signs of instability for many years.

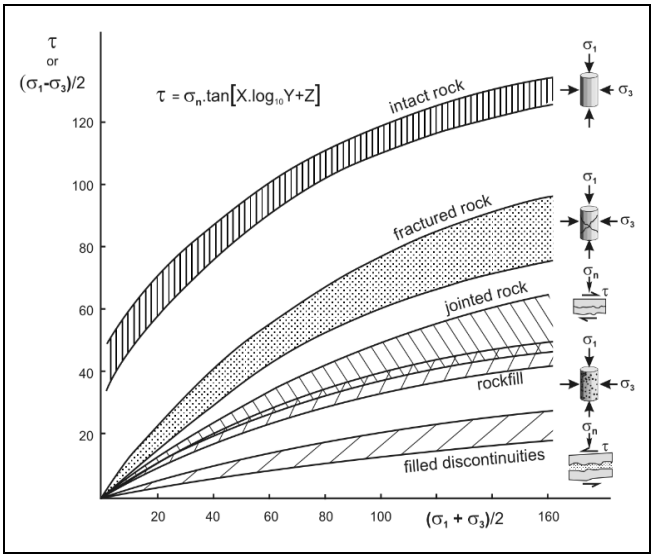

Figure 49. A shear strength diagram which symbolizes the strength components of rock masses, in other words: intact bridges, new fractures, joints, filled discontinuities.

The shear strength of rock masses should not logically be based on an algebraically altered intact rock strength criterion, requiring the most extraordinary set of algebra and semi-empiricism. It should be based on the majority component of rock mass strength: the joints.

REFERENCES

Addis, M.A., Barton, N., Bandis, S.C. & Henry, J.P. 1990. Laboratory studies on the stability of vertical and deviated boreholes. 65th Annual Technical Conference and Exhibition of the Society of Petroleum Engineers, New Orleans, September 23-26, 1990.

ASG, 2010. NATM: The Austrian Practice of Conventional Tunnelling.

Aydan, Ö. And Ulusay, R. 2016. Rock engineering evaluation of antique rock structures in Cappadocia Region of Turkey. Rock Mechanics and Rock Engineering: From the Past to the Future. Ulusay et al. (Eds), Taylor and Francis.

Barton, N. 1994. A Q-system case record of cavern design in faulted rock. 5th Int. Rock Mechanics and Rock Engineering Conf., Tunnelling in difficult conditions, Torino, Italy, pp. 16.1-16.14.

Barton, N. & Grimstad, E. 1994. The Q-system following twenty years of application in NMT support selection. 43rd Geomechanics Colloquy, Salzburg. Felsbau, 6/94. pp. 428-436.

Barton, N. & Warren, C. 1996. Rock mass classification of chalk marl in the UK Channel Tunnels. Channel Tunnel Engineering Geology Symposium, Brighton, September 1995.

Barton, N. 2002. Some new Q-value correlations to assist in site characterization and tunnel design. Int. J. Rock Mech. & Min. Sci. Vol. 39/2:185-216.

Barton, N. & Infanti, N. 2004. Unexpected stress problems in shallow basalts at the Ita hydroelectric power project in S.E. Brazil. Proc. ARMS 2004 : 3rd Asian Rock Mechanics Symposium, Kyoto.

Barton, N. 2007. Future directions for rock mass classification and characterization – Towards a cross-disciplinary approach. Invited lecture. Proc. of *1st US-Canada Rock Mech. Symp*., Vancouver.

Barton, N. 2009. Differential Weathering and Adverse Discontinuities were the Apparent Causes of a Tragic Metro Accident in Brazil. *Proc. Int. Conf. on Rock Joints and Rock Masses*, Tucson, Arizona.

Barton. N. 2010. Low Stress and High Stress Phenomena in Basalt Flows. Keynote paper. *3rd International Workshop on Rock Mechanics and Geo-Engineering in Volcanic Environments.* Tenerife.

Barton, N. & Grimstad, E., 2014. Q-system - an illustrated guide following forty years in tunnelling. Web site www.nickbarton.com, 43 pages, 79 figures and photos.

Barton, N. and E. Quadros, 2015. Anisotropy is everywhere, to see, to measure and to model. Rock Mechanics and Rock Engineering, Rock Mechanics and Rock Engineering. July 2015, Volume 48, 1323-1339.

Bray, J.W. 1967. A study of jointed and fractured rock. Part I. Fracture patterns and their failure characteristics. *Felsmechanik, V/2-3, 117-136.*

Grimstad, E. & Barton, N. 1993. Updating of the Q-System for NMT. Proceedings of the International Symposium on Sprayed Concrete - Modern Use of Wet Mix Sprayed Concrete for Underground Support, Fagernes, 1993, (Eds Kompen, Opsahl and Berg. Norwegian Concrete Association, Oslo, 46-66.

Hoek, E. 1991. When is a design in rock engineering acceptable? 1st Müller Lecture of ISRM. Proc. of 7th Congress, Aachen. Vol. 3, 1485-1497.

Kaşmer, Ö, Ulusay, R. and Geniş, M., 2013. Assessments on the stability of natural slopes prone to toe erosion, and man-made historical semi-underground openings carved in soft tuffs at Zelve Open-Air Museum (Cappadocia, Turkey). Engineering Geology 158 (2013) 135-158.

Martin, C.D., Kaiser, P.K. & McCreath, D.R. 1999. Hoek–Brown parameters for predicting thedepth of brittle failure around tunnels. Can. Geotech. J. 36, 136-151.

Shen, B., Stephansson, O. & Rinne, M., 2013. *Modelling Rock Fracturing Processes: A Fracture Mechanics Approach Using FRACOD.* Springer, 173p.

Stacey, T.R. 1981. A simple Extension Strain Criterion for Fracture of Brittle Rock. *Int. J. Rock Mech. Min. Sci. & Geomech. Abstr.* 18, 469-474.

Ward, W.H., P. Todd and N.S.M.Berry. (1983). The Kielder Experimental Tunnel: Final Results. Geotechnique 33, 3, 275-291.